

**Combined bioreduction and volatilization of SeVI by
Stenotrophomonas bentonitica: Formation of trigonal
selenium nanorods and methylated species**

RUIZ-FRESNEDA, Miguel A., FERNÁNDEZ-CANTOS, María V., GÓMEZ-BOLÍVAR, Jaime, ESWAYAH, Abdurrahman S., GARDINER, Philip H.E. <<http://orcid.org/0000-0002-2687-0106>>, PINEL-CABELLO, Maria, SOLARI, Pier L. and MERROUN, Mohamed L.

Available from Sheffield Hallam University Research Archive (SHURA) at:
<https://shura.shu.ac.uk/31158/>

This document is the Accepted Version [AM]

Citation:

RUIZ-FRESNEDA, Miguel A., FERNÁNDEZ-CANTOS, María V., GÓMEZ-BOLÍVAR, Jaime, ESWAYAH, Abdurrahman S., GARDINER, Philip H.E., PINEL-CABELLO, Maria, SOLARI, Pier L. and MERROUN, Mohamed L. (2023). Combined bioreduction and volatilization of SeVI by *Stenotrophomonas bentonitica*: Formation of trigonal selenium nanorods and methylated species. *The Science of the total environment*, 858 (Pt 2): 160030. [Article]

Copyright and re-use policy

See <http://shura.shu.ac.uk/information.html>

Research paper

**Combined bioreduction and volatilization of Se^{VI} by
Stenotrophomonas bentonitica: formation of trigonal selenium
nanorods and methylated species**

Miguel A. Ruiz-Fresneda^{1,*}, María V. Fernández-Cantos^{1,#}, Jaime Gómez-Bolívar¹,
Abdurrahman S. Eswayah², Philip H. E. Gardiner³, Maria Pinel-Cabello¹, Pier L. Solari⁴,
Mohamed L. Merroun¹

¹Department of Microbiology, University of Granada, Granada, Spain

²Biotechnology Research Centre, Tripoli, Libya

³Biomolecular Sciences Research Centre, Sheffield Hallam University, Sheffield, UK

⁴MARS Beamline, Synchrotron SOLEIL, L'Orme des Merisiers, Saint-Aubin, Gif-sur-Yvette
Cedex, France

[#]Present address: Department of Molecular Genetics, Groningen Biomolecular Sciences and
Biotechnology Institute, University of Groningen, Nijenborgh 7, 9747AG Groningen, The
Netherlands.

*Corresponding author: Miguel Angel Ruiz-Fresneda. Email: mafres@ugr.es

Abstract

Nowadays, metal pollution due to the huge release of toxic elements to the environment has become one of the world's biggest problems. Bioremediation is a promising tool for reducing the mobility and toxicity of these contaminants (e.g. selenium), being an efficient, environmentally friendly, and inexpensive strategy. The present study describes the capacity of *Stenotrophomonas bentonitica* to biotransform Se^{VI} through enzymatic reduction and volatilization processes. HAADF-STEM analysis showed the bacterium to effectively reduce Se^{VI} (200 mM) into intra- and extracellular crystalline Se^0 nanorods, made mainly of two different Se allotropes: monoclinic (*m*-Se) and trigonal (*t*-Se). XAS analysis appears to indicate a Se crystallization process based on the biotransformation of amorphous Se^0 into stable *t*-Se nanorods. In addition, results from headspace analysis by gas chromatography-mass spectrometry (GC-MS) revealed the formation of methylated volatile Se species such as DMSe (dimethyl selenide), DMDSe (dimethyl diselenide), and DMSeS (dimethyl selenenyl sulphide). The biotransformation pathways and tolerance are remarkably different from those reported with this bacterium in the presence of Se^{IV} . The formation of crystalline Se^0 nanorods could have positive environmental implications (e.g. bioremediation) through the production of Se of lower toxicity and higher settleability with potential industrial applications.

Keywords: bacteria, selenate, reduction, bioremediation, nanorod, volatilization

1. Introduction

Exhaustive investigations in the past decade have shed light on the occurrence of a wide diversity and distribution of microorganisms recognized as capable of selenium (Se) oxyanion bio-transformations (Avendaño et al. 2016; Presentato et al. 2018; Ojeda et al. 2020). Oxidation, reduction, and volatilization have been reported as the main pathways involved in the biotransformation of the different Se oxidation states: selenate (Se^{VI}), selenite (Se^{IV}), elemental Se (Se^0), and selenide ($\text{Se}^{\text{II-}}$). Selenate and selenite are known to be environmentally hazardous due to their high solubility, mobility, and bioavailability, while Se^0 is insoluble and less toxic. A few studies have reported the oxidation of reduced Se species by microorganisms (Dowdle and Oremland 1998; Losi and Frankenberger 1998; Luo et al. 2022; Nancharaiah and Lens 2015). However, microbial oxidation of Se is not usually considered to be of major relevance for the environment because of the low rates at which these reactions occur (Eswayah et al. 2016). Se volatilization is a biotransformation process now considered as a promising mechanism for bioremediation purposes. Some selenium-resistant microorganisms are able to volatilize Se through biomethylation processes (Eswayah et al. 2017). Selenium methylated compounds such as DMSe or DMDSe reportedly present limited bioavailability, toxicity, and solubility in comparison to Se oxyanions (Doran 1982; Hasanuzzaman et al. 2020; Ranjard et al. 2003). Finally, the reduction of oxidized and toxic forms of Se (Se^{VI} and Se^{IV}) to Se^0 nanoparticles (NPs) has been extensively studied (Martínez et al. 2020; Tugarova et al. 2020). Even though changes in the oxidation state —hence bioreduction— have been confirmed in many cases, the specific mechanisms, regulators, and biochemical pathways involved in this process have not yet been fully elucidated. To date, the number of Se^{IV} -reducing microbial isolates is considerably higher than Se^{VI} -reducing ones, which generally require a two-step process in which Se^{IV} act as an intermediate product. Therefore, both volatilization and reduction are potential mechanisms to be used in bioremediation of contaminated environments since they involve the removal of toxic Se species. However, there is still much to be investigated about bioremediation and its possible in-situ application, so any step forward in its research would be of crucial importance in the search for an effective strategy.

Of industrial and environmental interest is the type, form, and location of the Se^0 NPs produced after Se bioreduction. Indeed, a wide array of nanoparticle shapes (spheres, nanotubes, nanorods, etc.), structures (amorphous, trigonal, monoclinical, etc.), sizes, and cellular locations has been described. This suggests that there is no unique Se biotransformation mechanism. Elemental Se exists in nature in several allotropic forms including both amorphous (*a*-Se) and crystalline varieties (monoclinic (*m*-Se) and trigonal Se (*t*-Se)). Amorphous Se tends to change to the more stable crystalline Se by heating, use of chemical reagents, and other physico-

chemical methods (Zhang et al. 2012). However, some bacteria can transform *a*-Se to *m*-Se and *t*-Se at room temperature and without the use of additional reactive (Komova et al. 2018; Ruiz-Fresneda et al. 2020; Pinel-Cabello et al. 2021). Indeed, some authors propose that *a*-Se nanospheres are released from the cell and transformed to Se crystal nanostructures of different shapes (Wang et al. 2010; Ruiz-Fresneda et al. 2018; Ruiz-Fresneda et al. 2020). For example, the bacterium *Stenotrophomonas bentonitica* have been recently identified to reduce Se^{IV} to Se⁰ nanospheres (*a*-Se), different crystalline nanostructures (*m*-Se and *t*-Se), and with the formation of volatile methylated Se (Ruiz-Fresneda et al. 2020). They proposed a transformation mechanism from *a*-Se to Se crystals including the intracellular synthesis of the *a*-Se nanospheres and their subsequent release, aggregation, and transformation in the extracellular space. Unfortunately, it remains unclear how these relatively huge nanospheres—in comparison with the cell size—are formed, assembled, released, and transformed. It is likely that many unknown proteins, enzymes, and transport complexes may be involved. Interestingly, results from recent proteomic studies indicate the possible role of specific proteins in Se^{IV} reduction, including RND (resistance-nodulation-division) transport systems, and glutathione reductase (Pinel-Cabello et al. 2021), which has been found to be important in Se reduction in other bacterial species (Ni et al. 2015; Martínez et al. 2020).

The importance of Se crystal formation lies in the potential number of applications derived from it. For instance, crystalline Se has been described to be more settleable than *a*-Se (Lenz et al. 2009), which may be beneficial for the decontamination of Se polluted environments. Recent experiments in bioreactors highlight bioremediation as potential tool for contaminated water treatment (Dessi et al. 2016; Ojeda et al. 2020). Likewise, certain Se-reducing bacteria may play an important role in the immobilization of Se, positively affecting the safety of deep geological repositories (DGR) (Ruiz-Fresneda et al. 2018; Ruiz-Fresneda et al. 2019), the most accepted option for final disposal of radioactive residues. In addition, the utility of *t*-Se in many industrial and medical applications is well-known. *t*-Se is a photoconductor of broad spectral sensitivity, making it very useful in solar cells, photocells, rectifiers, photographic exposure meters, and xerography (Ibragimov et al. 2000; An et al. 2003; Zhu et al. 2019). From a medical standpoint, Se nanoparticles hold potential as antitumoral and antibacterial agents (Kuršvietienė et al. 2020; Filipović et al. 2021). It is worth mentioning that for many of the previous applications, nanoparticles must be crystalline, smaller than 100 nm, and as flawless as possible (An et al. 2003). Although many studies are reporting the bioproduction of selenium nanoparticles (SeNPs) through bacteria, archaea, plants, fungi, etc., there is still no optimized eco-friendly methodology applied to the industrial production of NPs. For this reason, any contribution to the field could be of great help in the search for an effective synthesis method.

The study presented here describes the mechanisms involved in the reduction of Se^{VI} by *S. bentonitica* as compared to those reported for Se^{IV} (Ruiz-Fresneda et al. 2018). This bacterium reduced Se^{VI} to extracellular and intracellular Se^0 nanorods (*m*-Se and *t*-Se) and methylated Se compounds. The results evidenced a different and novel Se^{VI} reduction mechanism entailing the formation of intracellular crystalline nanorods, never described before, with no observation of *a*-Se nanospheres. This study thus provides new information to be considered in the development of novel bioremediation strategies and tools. In addition, *S. bentonitica* is clearly identified as a candidate for environmentally friendly methodologies in *t*-Se nanorod fabrication.

2. Materials and methods

2.1. Bacterial species and growing conditions under Se^{VI} stress

The bacterium *Stenotrophomonas bentonitica* used in the present study was isolated from Spanish bentonite clays (Almeria, Spain) and selected based on previous genomic and metal interaction studies (Sánchez-Castro et al. 2017). The bacterial cells were grown aerobically in Luria-Bertani (LB) broth medium (tryptone 10 g/l, NaCl 10 g/l, and yeast extract 5 g/l and, pH 7.0 ± 0.2) at 28 °C and 180 rpm. Specifically, the cells were inoculated to an initial optical density (OD) of 0.1 at a wavelength of 600 nm for all the experiments. Se^{VI} tolerance by *S. bentonitica* was studied by growing the cells aerobically in liquid LB (25 ml) added with 50, 100, and 200 mM Se^{VI} at 28 °C by shaking at 180 rpm. Growth was quantified at different incubation times (0, 8, 24, 48, and 72 h) by calculating the cell protein content following the method employed by Ruiz-Fresneda et al. (2018, 2019, 2020) based on Bradford's reagent.

2.2. X-ray diffraction (XRD)

XRD analysis was used to identify the crystalline phase of the Se reduction products. For this purpose, high volumes of *S. bentonitica* cultures (500 ml) treated with different initial Se^{VI} concentrations (50, 100, 150, and 200 mM) were harvested after 24 h (10,000 x g for 10 min). Dried powder samples were obtained as indicated by Ruiz-Fresneda et al. (2018) and measured with a Bruker D8 Advanced diffractometer linked to a LINXEYE detector.

2.3. X-ray absorption spectroscopy (XAS) measurements

XAS is a synchrotron-based analytical technique widely employed for local chemical structure determinations of different materials, and hence can be successfully used to determine the structure and oxidation state of Se allotropes produced by the cells of *S. bentonitica* (Lopez-Fernandez et al. 2020). For XAS experiments, *S. bentonitica* cells were grown in LB supplemented with 200 mM Se^{VI}. After 17, 24 and 48 h of incubation the samples were collected, washed, dried, and powdered as described above in section 2.2. Subsequently, the powder samples were pressed on Kapton tape as indicated by Ruiz-Fresneda et al. (2020). Se standards (sodium selenate-Na₂SeO₄ (Se^{VI}), sodium selenite-Na₂SeO₃ (Se^{IV}), Se⁰ foil (*t*-Se) and selenium sulphide-SeS₂ (Se^{-II})) were prepared with cellulose forming small disks following the procedures of Ruiz-Fresneda et al. 2020. The XAS data of the experimental samples and Se standards were collected in fluorescence and transmission mode, respectively.

Selenium K-edge X-ray absorption spectra were measured at the MARS beamline (SOLEIL synchrotron facility in Paris, France), which is a bending magnet beamline for Multi Analyses on Radioactive Samples. The experimental setup and technical parameters behind the measurements were same as those followed in Ruiz-Fresneda et al. (2020); they are detailed in the **Supplementary Material 1.1**.

2.4. Electron Microscopy

The crystallographic/structural analysis and cellular location of the Se reduction products were analyzed by means of high-angle annular dark field scanning transmission electron microscopy (HAADF-STEM) fitted with energy dispersive X-ray (EDX), selected-area electron diffraction (SAED), and Fast Fourier Transform (FFT). The samples consisting of Se^{VI}-treated cells (150 and 200 mM Se^{VI}) were prepared as described in Merroun et al. (2005) after 24 and 48 h incubating, and subsequently examined under a HAADF-STEM microscope FEI TITAN G2 80-300 (University of Granada, Granada, Spain). The samples were further examined under FEG-ESEM (field emission gun environmental scanning electron microscopy) on a FEG-SEM Microscope FEI QEMSCAN 650F (University of Granada, Spain). The samples were prepared using the critical point drying method as described in Ruiz-Fresneda et al. (2018).

2.5. Gas Chromatography Mass Spectrometry (GC-MS).

GC-MS combined with thermal desorption (250°C) system was employed for the qualitative analysis of volatile Se-containing compounds released by *S. bentonitica* cells. To this end, the cells were incubated with 2 and 100 mM Se^{VI} in special conical flasks (QuickfitTM) capped with Suba-Seals (SigmaTM) rubber septa as described in Ruiz-Fresneda et al. (2020). Headspace gases were sampled and analyzed after 144 h of incubation as described previously (Eswayah et al. 2017). Se^{VI}-free cultures (biotic) and Se^{VI}-added media (abiotic) were employed as controls. All measurements were performed in duplicate.

3. Results and discussion

3.1. Selenate reduction and tolerance assays for *S. bentonitica*

The reduction of Se^{VI} was confirmed by the formation of red precipitates characteristic of Se^0 in Se^{VI} -treated cultures after 24 h of incubation (**Figure 1A**). The non-formation of such precipitates in Se^{VI} -untreated cultures (**Figure 1B**) and Se^{VI} -treated media (biotic and abiotic controls) (**Figure 1C-D**) indicated that Se^{VI} reduction is a biological process mediated by the cells of *S. bentonitica*. Interestingly, the formation of the reddish colour and thus of Se^0 nanoparticles of interest in the Se^{VI} -treated cultures was only observed at high initial concentrations (100-200 mM), but not at lower initial concentrations (10 and 50 mM) (**Figure S1-Supplementary Material**). These results suggest that Se^{VI} would not exert a high toxic effect upon the cells of *S. bentonitica* at low metalloid concentrations. For this reason, 200 mM Se^{VI} was selected as initial concentration for most of the experiments. It is noteworthy that transcriptomic studies showed that the cells respond metabolically differently with Se^{VI} concentration (Pinel, 2021). Thus, genes encoding for efflux transporters and several oxidoreductases were clearly overexpressed at concentrations below 200 mM (e.g. 50 mM). In this case, where no red precipitation is present, the cells would be capable of reducing Se^{VI} to Se^{IV} , which is removed most probably by these transporters to the extracellular space. For all the above reasons, it is quite probable that an additional resistance mechanism apart from reduction —such as volatilization, which does not trigger a colour change in the cultures— is involved.

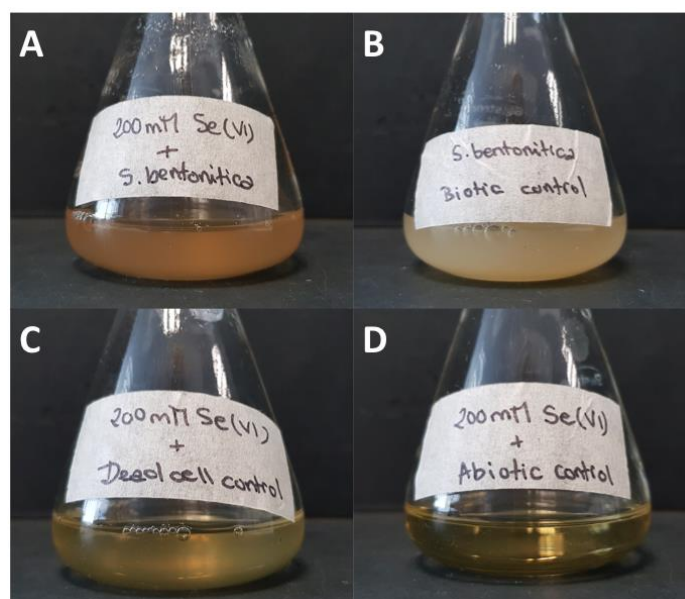


Figure 1. Cultures of *Stenotrophomonas bentonitica* in LB broth medium with (A) and without 200 mM Se^{VI} (B) after 24h incubation. Dead cell (C) and abiotic (D) controls were both supplemented with 200 mM Se^{VI} .

The toxicity of Se^{VI} was evaluated by determining the bacterial growth rate under different Se^{VI} concentration levels (0, 50, 100, and 200 mM). As can be seen in **Figure 2**, cell growth curve of the biotic control in the absence of selenate (0 mM Se^{VI}) showed a normal pattern of bacterial growth. Considerable differences in cell growth in the presence of 50 and 100 mM during the first 48 h confirmed the toxicity of Se^{VI} , with an observable small delay in the lag phase of growth of about 8 h. However, after 48 h growing, no differences were appreciated between the control and these Se^{VI} concentrations. When the cells were grown under 200 mM Se^{VI} , the growth rate is clearly affected. The lag and the exponential phases are prolonged until 24 and 48 h, respectively. However, despite the evident toxic effect, the cells were able to reach growth levels compare with the control after 72 h, revealing the capacity of *S. bentonitica* to tolerate high concentration levels of Se^{VI} . All these observations suggest that the cells cope with the toxicity of Se^{VI} through several mechanisms depending on concentrations, including enzymatic reduction, export of Se^{VI} by oxidoreductases and transporters, and/or mitigation of oxidative stress by enzymes such as glutathione S-transferase (Pinel, 2021). The bacterium of study was previously characterized as efficiently reducing Se^{IV} at lower initial concentrations (0.1 to 2 mM) than those employed here for Se^{VI} (Ruiz-Fresneda et al. 2020) —in their study, *S. bentonitica* growth rate was strongly affected by Se^{IV} at 2 mM. This finding reveals that *S. bentonitica* cells are more resistant to Se^{VI} than to Se^{IV} .

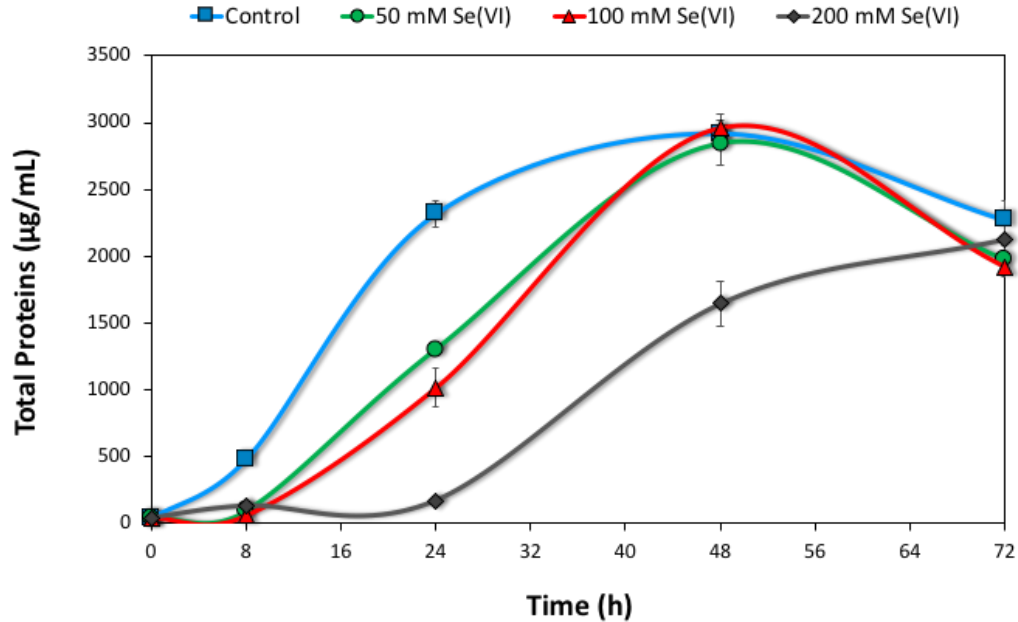


Figure 2. Growth profile of *Stenotrophomonas bentonitica* at different concentrations of Se^{VI} : 0, 50, 100, and 200 mM Se^{VI} .

Although Se is usually present in nature at relatively low concentrations, there is a growing increase in the release of this contaminant into the environment in the last years. For instance, Chang et al. (2019) reported concentrations up to 7007 mg/kg in seleniferous soil areas in

central China, similar to those tested in the present study. In addition, several plant species such as *Astragalus L.*, *Oonopsis (Nutt.) Greene*, *Oryzopsis Michx.*, *Xylorhiza Nutt.*, or *Mentzelia L.* (Presser, 1999), can accumulate from 1000 to 10,000 mg/kg selenium (dry weight), being a potential source of Se in the environment. There is no report in the literature with similar results with bacterial strains tolerating and reducing such high concentrations. In this regard, *S. bentonitica* is presented herein as a potential microorganism to be used for decontamination of highly polluted environment.

3.2. XRD analysis

The structure of the Se^{VI}-reduction products was characterized using the XRD technique. The XRD patterns of the samples obtained after 24 h of incubation show the main peaks characteristic of crystalline *t*-Se (COD-9008579) at 2θ values of 23.4°, 29.7°, 41.1°, 43.6° and 45.3°, and 51.7° (**Figure 3**), corresponding to the crystal planes (1 0 0), (0 1 1), (1 1 0), (1 0 2), (1 1 1), and (0 2 1), respectively, for initial Se^{VI} concentrations of 100, 150, and 200 mM. For 50 mM Se^{VI}, no peaks were observed, most probably due to the lower toxicity exerted by this element at this concentration and non-formation of Se crystals. Interestingly, for 100 and 150 mM concentrations, peaks belonging to the *t*-Se phase can be observed in the absence of a colour change. This suggests that the reduction rate increased, but not enough to produce the characteristic red precipitates. No differences in the diffraction patterns were observed when varying the incubation time from 17 to 48h at the same concentration (200 mM Se^{VI}) (**Figure S2-Supplementary Material**)

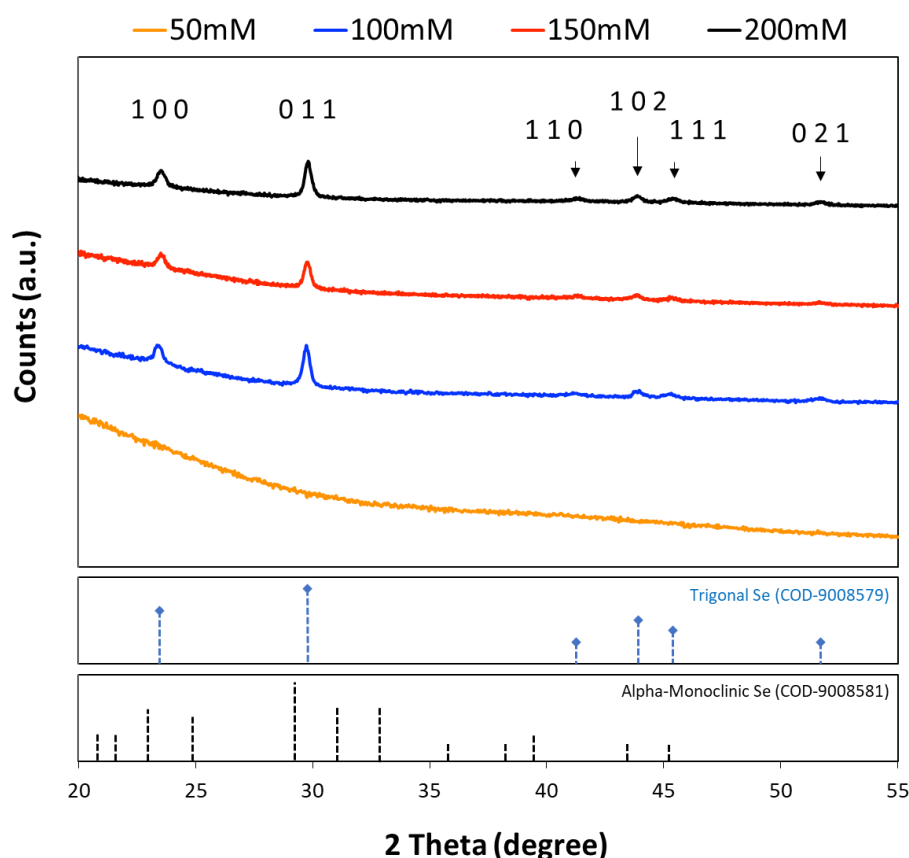


Figure 3. X-ray diffraction patterns of cultures of *S. bentonitica* supplemented with 50, 100, 150, and 200 mM Se^{VI} after 24h of incubation. Peaks for Se with a *t*-Se were detected for cultures supplemented with 100, 150, and 200 mM as indicated the corresponding crystal planes (black arrows). X-ray reflections of *t*-Se (COD-9008579) and m-Se (COD-9008581) obtained from Crystallography Open Database (<http://www.crystallography.net/cod/>) are shown at the bottom.

3.3. FEG-ESEM and HAADF-STEM analysis

A combination of FEG-ESEM and STEM/HAADF was used to determine the structure and physical properties of the Se^{VI} reduction products needed for the elucidation of biological Se^{VI} biotransformation by the cells of *S. bentonitica*. Three-dimensional (3D) images obtained by a FEG-ESEM system showed the presence of electron-dense nanorods mostly in the intracellular space of the cells, but also extracellularly, after 24 and 48 h of incubation with 150 (**Figure 4A-B**) and 200 mM Se^{VI} (**Figure 4C-E**). Energy Dispersive X-Ray Analysis (EDX) clearly showed these nanostructures to be composed of Se in addition to small peaks of sulfur (S) (**Figure 4F**). The presence of both Se and S suggest the participation of S-containing compounds as intermediates and biocatalysts in Se^{VI} reduction. A set of biochemical pathways implicating S-doped molecules such as glutathione (GSH), glutathione reductase (GR), glutathione peroxidase (GP), or thioredoxin reductase (TrxR) in formation of Se⁰ through a series of redox reactions have been widely reported before (Xu and Barton 2013; Eswayah et al. 2019). Interestingly,

organic Se molecules such as selenocysteine amino acids are known to be essential in the catalytic activity of TrxR or GP forming a redox active disulfide bond in the active site (Hawkes and Alkan 2010). Both enzymes GR and TrxR could be involve in reduction to Se⁰ in *S. bentonitica* since the genes encoding them are present in its genome (accession number: MKCZ000000000).

The formation of Se nanoparticles having diverse morphologies is widely described (Presentato et al. 2018; Fischer et al. 2020). Yet to the best of our knowledge, it is the first time that tubular-shaped Se nanoparticles produced from a Se^{VI} reduction process could be observed intracellularly. Interestingly, these relatively big and long nanorods can be observed intracellularly without signs of cell lysis. The strain of study *S. bentonitica* has been highlighted in recent years for its ability to reduce Se^{IV} to Se⁰ forming amorphous Se nanospheres and trigonal nanorods (Ruiz-Fresneda et al. 2018; Ruiz-Fresneda et al. 2020). Based on such findings, the authors invoked a biotransformation mechanism whereby intracellular amorphous Se nanospheres are released to the extracellular space during the first 24-72 h, followed by transformation to different Se allotropes (monoclinic and trigonal) after 144 h. Other authors suggest a similar transformation pathway in different bacterial species: *Bacillus subtilis* and *Zoogloea ramigera* (Wang et al. 2010; Srivastava and Mukhopadhyay 2013). In the present study, however, Se nanorod formation was observed at 24 h and mainly located intracellularly, evidencing that different transformation and interaction processes may occur in *S. bentonitica* when the initial Se source is Se^{VI} instead of Se^{IV} (Ruiz-Fresneda et al. 2018). Our findings suggested the reduction and Se nanorod synthesis occurred intracellularly and are then released somehow. Cytoplasmic enzymes from several microorganisms (*Burkholderia fungorum* 95, *Burkholderia fungorum* DBT1, or *Bacillus mycoides* SeITE01) have been reported to be involved in Se^{IV} reduction (Khoei et al. 2017; Lampis et al. 2014). Lampis et al. (2014) proposed thioredoxin reductase (TrxRed) systems and thiol-containing molecules with redox activity in Se⁰ nanoparticle formation of *B. mycoides* SeITE01. Different export mechanisms have been hypothesized by several authors causing SeNPs leak outside the cells. Some of them suggested the SeNPs are released after cell death and lysis (Lampis et al. 2014). A few extracellular nanorods were produced in our case, but no signs of bacterial lysis were observed after 24h. Other export system proposed were based on secretion of the NPs through outer membrane vesiculation and encapsulation (Kulp et al. 2010). For example, the gram-negative bacterium *Thauera selenatis* use the protein Se factor A (SefA) for SeNPs binding, stabilization, and secretion to the extracellular space (Debieux et al 2011). Further upcoming investigations will help to elucidate the synthesis pathway for *S. bentonitica*.

From an industrial point of view, the faster production of crystalline SeNPs presented herein points out a most promising crystalline NPs synthesis process compared to others. Wang et al. (2010) reported a more rapid formation of crystalline Se nanorods (12 h) by *B. subtilis*, but with the help of reactive agents such as ethanol. Similar Se tubular structures were produced by anaerobic granular sludge after 18 h at 55°C (Jain et al. 2017). Interestingly, *S. bentonitica* can form *t*-Se nanorods without the use of chemicals and room temperature, providing a more ecologic and less expensive synthesis method. In terms of quantitative data, *S. bentonitica* is highlighted herein as promising SeNPs producer as observed in the micrographs of thin sections with up to 6 nanorods in a single cell (**Figure 5**).

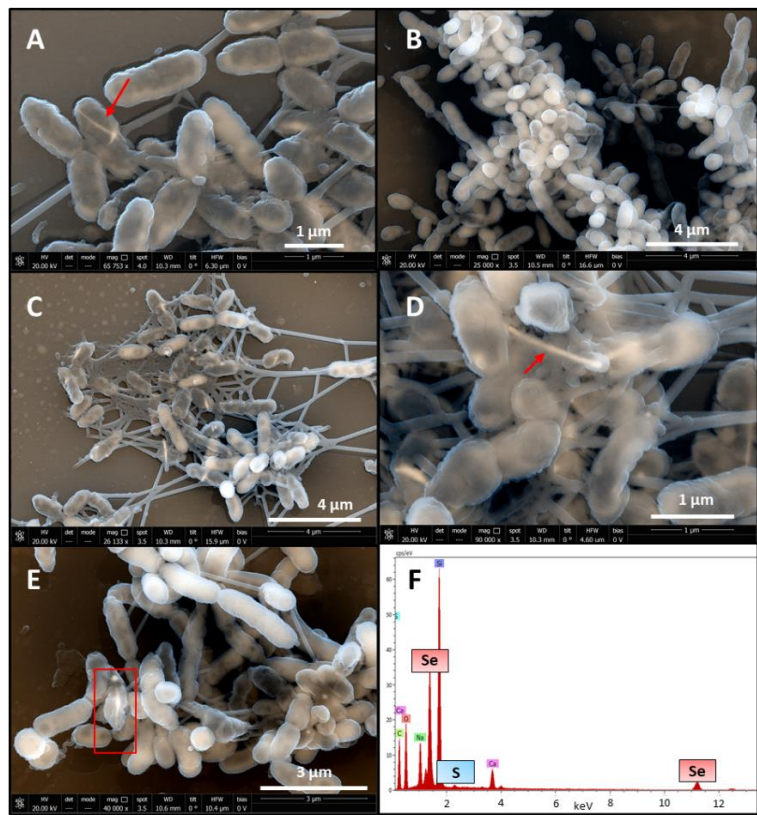


Figure 4. FEG-ESEM of cultures of *S. bentonitica* supplemented with 150 mM of Se^{VI} after 24 (A) and 48h (B), and with 200 mM of Se^{VI} after 24 (C and D) and 48h (E). EDX analysis of a single nanorod (highlighted area in panel in E) confirmed the presence of Se (F).

Ultrathin sections observed with an HAADF-STEM system allowed for further structural characterization of the Se nanostructures produced by *S. bentonitica*. By means of this technique we again observed that the predominantly Se nanostructure was found intracellularly in the form of nanorods (**Figure 5A**). Element-distribution maps indicated the presence of both Se and S in the nanorods (**Figure 5B-D**), strongly supporting the possible relevance of thiol-containing proteins in the reduction pathway.

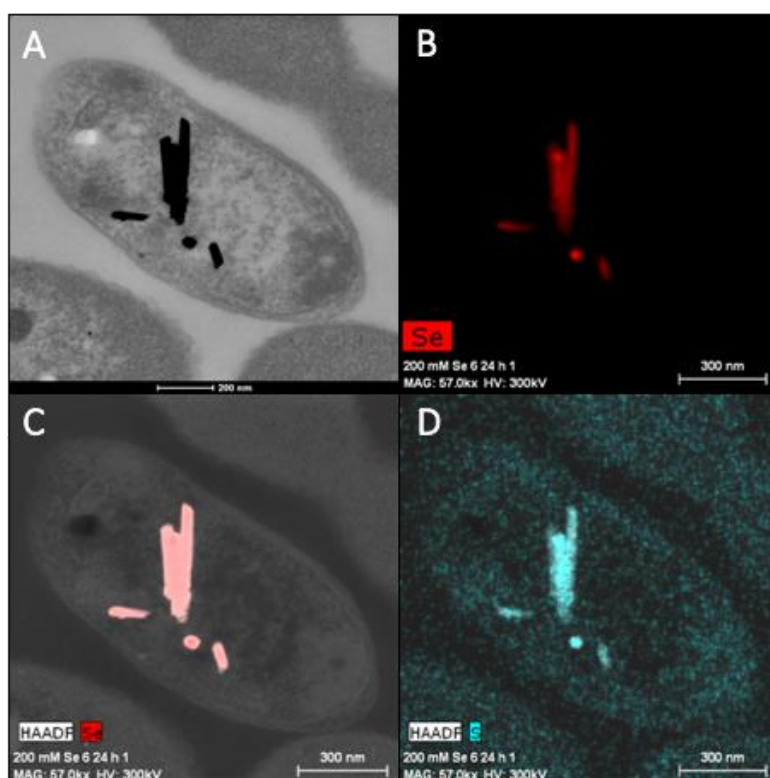


Figure 5. HAADF-STEM micrographs of a thin section showing Se nanostructures produced by *S. bentonitica* after 24 h of incubation with Se^{VI} (A). EDX element-distribution maps showing their Se and S elemental composition (B-D).

A combination of tools of the HAADF-STEM system—including SAED (Selected Area Electron Diffraction), FFT (Fast-Fourier Transform), and STEM high resolution (HRTEM)—attested to the crystalline nature of the Se nanostructures. SAED and FFT patterns from a selected Se nanorod revealed signs of crystallization (**Figure 6A-C**); specifically, three different d-spacings of 0.29, 0.37, and 0.48 nm could correspond to crystal planes of monoclinic-Se (*m*-Se) (Pinel-Cabello et al. 2021) (**Figure 6B**). The space lattices 0.29 and 0.37 nm are characteristic as well in trigonal Se (*t*-Se) according to the American Mineralogist Crystal Structure Database (<http://rruff.geo.arizona.edu>) [accessed December, 2021]. Yet the detection of the 0.48 nm d-spacing confirmed the monoclinic structure of the nanorods. Similar results were obtained recently for Se nanorods produced by *S. bentonitica* contacted with Se^{IV} (Pinel-Cabello et al. 2021). HRTEM analyses, along with the FFT from a nanorod selected area, agree with the SAED pattern, revealing the presence of 0.29-0.3 and 0.38 nm lattice spacings (**Figure 6C-F**). As mentioned above, these spacings could correspond to different crystal planes of both *m*-Se and *t*-Se. More specifically, the d-spacing of 0.3 nm could correspond to planes (1 0 1 or 0 1 1) of *t*-Se and many different planes of *m*-Se. The d-spacing of 0.37 nm may correspond to the plane (1 0 0) of *t*-Se, and (0 2 2) or (4 0 0) of *m*-Se. Therefore, the existence of *t*-Se should not be discarded since common d-spacings (0.3 and 0.38 nm) between *t*-Se and *m*-Se were

observed. Even the co-existence of mixed crystal phases in one same nanocrystal is possible in our Se nanostructures, as reported before for Sn nanoparticles (Haq et al. 2019). In fact, *t*-Se was previously detected in our samples with XRD (see section 3.2.). Naturally, XRD is a more representative and precise technique, as the bulk sample is measured, whereas under HAADF-STEM some selected crystals were analyzed. Ultimately, these results could indicate the biotransformation of *m*-Se (as a transitional allotropic form) to *t*-Se, as was reported for Se^{IV} (Ruiz-Fresneda et al. 2018). Still, the results clearly underline the importance of a multidisciplinary approach, combining microscopic and spectroscopic techniques, to exhaustively characterize nanoparticle structures.

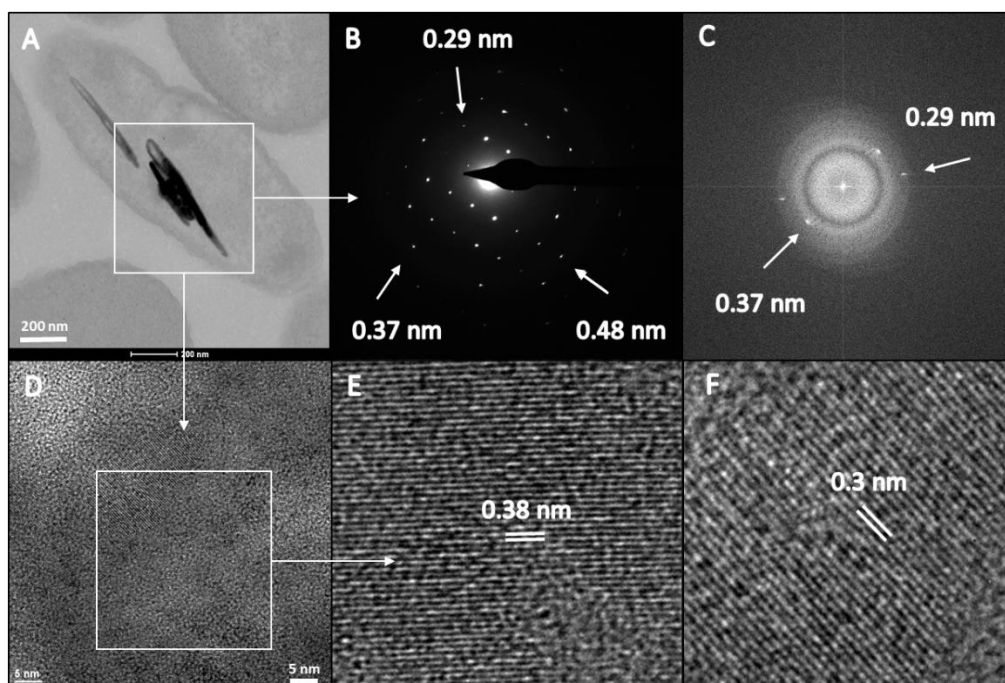


Figure 6. HAADF-STEM micrograph of Se nanostructures produced by *S. bentonitica* incubated with 200 mM Se^{VI} for 24 h (A). SAED pattern (B), FFT pattern (C), and HRTEM image (D) derived from a single nanostructure (highlighted area in panel A). Magnified HRTEM images (E and F) corresponding to highlighted area in D.

3.4. XAS analysis

X-ray absorption spectroscopy (XAS) spectra of the Se^{VI}-reduction products obtained after 17, 24, and 48 h of incubation with *S. bentonitica* (200 mM Se^{VI} as initial concentration) provided more detailed structural information concerning the local coordination environment, as well as the oxidation state of the Se in the studied samples. The X-ray absorption near-edge structure (XANES) region clearly showed that the local coordination of Se is dominated by Se⁰ at all incubation times, as indicated by the maximum peak positions obtained at 12659.3 eV, 12659.3 eV, and 12659.2 eV after 17, 24, and 48h incubating (**Figure 7A**) (**Figure S3 and S4-**

Supplementary Material). Generally, most of the bio-reduced SeNPs in solid form consisted of Se in the zero-valent oxidation state (Zhang et al. 2012; Vogel et al. 2018; Ruiz-Fresneda et al. 2020).

The extended X-ray absorption fine structure (EXAFS) spectra of the Se^{VI}-reduction products and Se foil (as Se⁰ reference compound), along with their corresponding Fourier transforms (FT) and fit parameters of the obtained spectra, are respectively presented in **Figure 7B-C**, **Figure S5-Supplementary Material**, and **Table 1**. FT peak distances are reported in units of Å and are expressed as $R + \Delta R$. The fit of the EXAFS spectra of the 3 experimental samples indicated the presence of one Se-Se coordination shell at a bond distance of about $2.35\text{--}2.37 \pm 0.02\text{Å}$ (**Table 1**). In previous XAS analyses obtained for the Se nanostructures produced by *S. bentonitica* with Se^{IV} this parameter ranged between 2.33 and 2.34 Å and were attributed to amorphous Se in view of the literature (Eswayah et al. 2017; Vogel et al. 2018; Ruiz-Fresneda et al. 2020). Slight increases of Se-Se bond distance values could indicate a crystallization process, while slight decreases in this frame point to an amorphization. Such is the case of the experiments by Zhao et al. (2004) and Breynaert et al. (2008), who found an amorphization process of crystalline Se upon a decrease from 2.37 to 2.35 Å. The increase of the Se-Se bond distances with incubation time found in our samples accordingly suggests a heightened structural order and therefore crystallization of Se⁰ over time. In view of the literature discussed above, the bond distances of 2.35 and 2.36 Å found after 17 and 24 h could correspond to a mixture of amorphous and trigonal Se, while the value of 2.37 Å found for 48 h samples might mark a Se crystalline phase mainly as trigonal Se (Zhao et al. 2004; Breynaert et al. 2008). However, our results are not conclusive about a dependent time crystallization process.

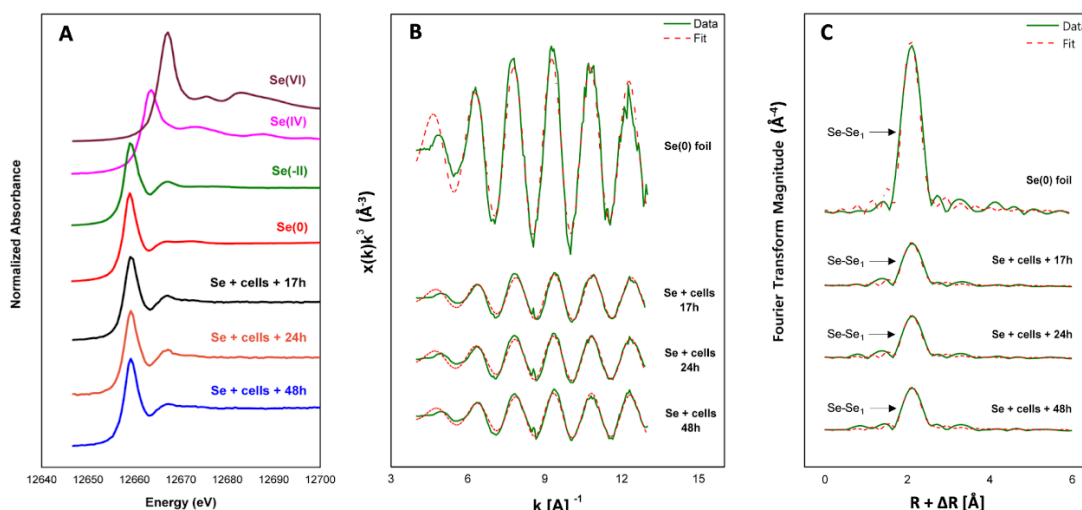


Figure 7. XANES (A), EXAFS (B), and their corresponding FT spectra (C) of Se reference compounds [Se^{VI} (Na₂SeO₄), Se^{IV} (Na₂SeO₃), Se⁰ (Se foil), and Se^{-II} (SeS₂)] and *S. bentonitica* samples incubated with 200 mM Se^{VI} at different incubation times (17, 24, and 48 h).

422

Table 1. EXAFS structural parameters of the Se foil and the Se^{VI}-reduction products.

Sample	Shell	N ^a	R[Å] ^b	σ ² [Å ²] ^c	ΔE[eV]
Se foil	Se-Se ₁	3.3 ± 0.2	2.37	0.0043	-5.6
Se ^{VI} - Cells-17h	Se-Se ₁	0.7 ± 0.1	2.35	0.0031	-3.1
Se ^{VI} - Cells-24h	Se-Se ₁	0.7 ± 0.1	2.36	0.003	-3.8
Se ^{VI} - Cells-48h	Se-Se ₁	0.6 ± 0.1	2.37	0.0028	-1.2

423

^a Errors in coordination numbers are ±25% and standard deviations as estimated by EXAFSPAK

424

^b Errors in distance are ±0.02 Å

425

^c Debye-Waller factor

426

427

3.5. Biological production of volatile Se compounds

428

429

Headspace analysis using GC-MS of extracted volatiles from 100 mM Se^{VI}-treated cultures indicated the formation of dimethyl selenide (DMSe), dimethyl diselenide (DMDSe) and dimethyl selenenyl sulphide (DMSeS) by the cells after 144 h incubating (**Figure 8**). In contrast, no volatile Se-containing species were detected in biotic and abiotic controls (**Figure S6-Supplementary Material**). The Se^{VI} initial concentration of 100 mM was selected for this analysis to increase the amount of volatiles that are produced. At this concentration, trigonal Se⁰ red precipitates derived from reduction processes were not as observable as for 200 mM, suggesting that other interaction mechanisms such as volatilization may have happened. The formation of Se volatile compounds presented herein revealed that volatilization is involved as a biotransformation mechanism in *S. bentonitica*, in addition to reduction. It is worth noting that no Se volatile species were produced by the cells when the Se^{VI} initial concentration was 2 mM (**Figure 8**). This suggests, as discussed in previous sections, that a very high Se^{VI} initial concentration is needed to let biotransformation occur, whether for volatilization or reduction process.

443

444

Interestingly, this bacterium does not produce DMSe when amended with Se^{IV} instead of Se^{VI} (Ruiz-Fresneda et al. 2020), thereby suggesting a different biotransformation pathway depending on the oxidation state of Se, even in the same microorganism. Thus, the versatile role of *S. bentonitica* in Se volatilization depends on the physico-chemical conditions. Not only is the Se oxidation state important, but also the type of SeNPs produced can influence Se volatilization. Otsuka and Yamashita (2020) showed that the structural nature of SeNPs affects the Se volatilization rates in *P. stutzeri* NT-I, a bacterial strain producing higher amounts of DMDSe when amorphous SeNPs were used as substrate as opposed to crystalline SeNPs. The differences between the nanoparticles formed by *S. bentonitica* (nanospheres and nanorods from Se^{IV}; only nanorods with Se^{VI}) might therefore condition the volatile compounds produced.

450

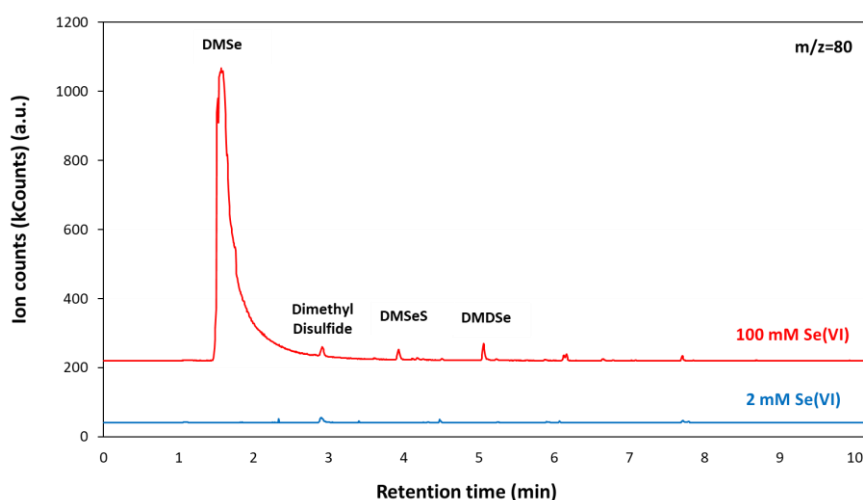


Figure 8. GC-MS chromatograms of the headspace gas of *S. bentonitica* cultures supplemented with Se^{VI} (2 and 100 mM) and after 144 h of incubation. All GC-MS chromatograms were obtained by selecting the 80 m/z ion specific for selenium.

No evident biochemical pathway is expounded in the literature to clearly explain how Se biovolatilization occurs. Most studies indicate that Se volatilization relies on reduction and methylation reactions when the initial form is a Se oxyanion. Accordingly, Se^{VI} or Se^{IV} are firstly reduced to Se⁰ or Se^{-II}, and subsequently methylated to DMSe (Eswayah et al. 2016). Methylation appears to be the most crucial or differential step, since a great number of reactions and intermediates —MeSeH, dimethyl disulfide (DMDS), dimethyl selenone, and Se aminoacids (SeMet and SeCys) have been suggested to be involved (Chasteen and Bentley 2003; Winkel et al. 2015). DMDS may be involved in the formation of DMSeS through its reaction with DMDSe (Chasteen 1993). The presence of these three compounds (DMDS, DMDSe, and DMSeS) in our samples comes to support this hypothesis as a possible mechanism active in *S. bentonitica* and the role of S-containing enzymes in the reduction process. Current evidence would suggest that the biochemical pathways responsible for Se volatilization remains to be elucidated, and it is likely that a variety of mechanisms could be involved depending on the given organism and the form of Se. From an environmental perspective, Se biomethylation is held to constitute a detoxification mechanism, as it enables the removal and transformation of toxic inorganic Se precursors toward less toxic methylated forms (Wilber 1980; Ranjard et al. 2003). This fact in itself points to a positive role of *S. bentonitica* in the bioremediation of Se contaminated sites. In the context of deep disposal of radioactive waste, however, Se production by *S. bentonitica* could compromise the integrity of such repositories by causing gas overpressure.

According to the results obtained both enzymatic reduction and volatilization are involved in Se^{VI} interactions with *S. bentonitica*. When Se^{VI} initial concentration is below 100 mM Se^{VI} is probably reduced to Se^{IV} by S-containing oxidoreductases (e.g. GR or TrxR) and then removed through efflux transporter to the extracellular space since no red precipitates were observable. This hypothesis agrees with preliminary transcriptomics studies (to be published). However, at concentrations over 100 mM the cells are capable of reducing Se^{VI} to Se^0 and $\text{Se}^{\text{-II}}$ volatile compounds due to these more stressful conditions. The experimental data suggested the reduction to Se^0 nanorods occurs intracellularly, before being released probably through vesicle secretion. The observation of organic matter surrounding some nanorods could be a sign of this (Figure 4D).

3.6. Environmental and industrial significance of the different Se allotropes produced

To sum up, the combination of spectroscopic and microscopic techniques showed the great potential of *S. bentonitica* to reduce Se^{VI} to Se^0 as crystalline nanorods with different allotropes (monoclinic and trigonal Se). The presence of *t*-Se crystalline phase in the biogenic nanorods was demonstrated by XRD. Lattice d-spacing values corresponding to *m*-Se could be observed by high resolution TEM analysis. These findings suggest a crystallization process from *m*-Se to the most thermodynamically stable phase *t*-Se. The XANES region of the XAS spectra confirmed the presence of the zero valent oxidation state of the Se reduction products, while the EXAFS region of the spectra showed the possible presence of different Se allotropes (amorphous, monoclinic, and trigonal). In addition, these Se nanorods could be stabilized by their interactions with organic matter as it was demonstrated for Se nanostructures derived from reduction of Se^{IV} by this bacterial strain (Ruiz-Fresneda et al. 2020). However, Se-C coordination shell does not seem to be visible in the EXAFS spectra of the studied samples. Therefore, further studies in the characterization of organic matter coating the Se nanorods should be performed using spectroscopic techniques like Infrared spectroscopy.

Ultimately, the results presented here point to *S. bentonitica* as an interesting bacterial model for bioremediation systems and for its potential as a new, green, and faster (only 24 h) way to produce crystalline SeNPs of substantial interest for industrial and medical applications.

4. Conclusions

The present work describes, for the first time, the ability of the bacterium *S. bentonitica* to reduce Se^{VI} to Se^0 nanorods and Se volatile compounds. The results clearly demonstrate a higher tolerance capacity of this bacterial species against Se^{VI} when compared to Se^{IV} experiments

performed in previous research. Differences in the structure, location, and formation speed of the Se reduction products when Se^{VI} is the initial source suggest a different biotransformation pathway than the one proposed for Se^{IV}. Still, more research is needed to fully understand the specific biotransformation processes. An exhaustive combination of spectroscopic and microscopic techniques applied here revealed important structural and chemical data, including the oxidation state and the crystalline phases of bio-reduced Se. The zero-valent oxidation state, tubular shape, and crystallinity of the Se nanostructures produced would uphold *S. bentonitica* as a potential bioremediation candidate in contaminated environments. The formation of volatile methylated species furthermore points to a positive role in the removal of toxic Se from polluted soils and waters, in terms of atmospheric bioremediation. Finally, *S. bentonitica* is put forth as a candidate for novel, environmentally friendly, and relatively quick Se nanorod fabrication.

CRedit authorship contribution statement

Miguel A. Ruiz-Fresneda: Conceptualization, Methodology, Validation, Formal Analysis, Investigation, Writing-Original Draft, Writing-Review & Editing, Visualization. **María V. Fernández-Cantos:** Conceptualization, Methodology, Validation, Formal Analysis, Investigation, Writing-Review & Editing. **Jaime Gómez-Bolívar:** Methodology, Validation. **Abdurrahman S. Eswayah:** Methodology, Validation. **Philip H. E. Gardiner:** Conceptualization, Resources, Writing-Review & Editing, Supervision. **Maria Pinel-Cabello:** Formal analysis, Writing-Review & Editing. **Pier L. Solari:** Methodology, Formal Analysis. **Mohamed L. Merroun:** Conceptualization, Methodology, Formal Analysis, Resources, Writing-Original Draft, Writing-Review & Editing, Supervision, Project Administration, Funding Acquisition.

Declaration of Competing Interest

Non-declared

Acknowledgements

This work was supported by grant RTI2018. 101548.B.I00 to M.L.M awarded by the Spain Ministry of Science and Innovation. The authors acknowledge the assistance of Maria del Mar Abad Ortega and Concepción Hernández Castillo (Centro de Instrumentación Científica, University of Granada, Spain) for their help with microscopy analysis and sample preparation.

References

- An C, Tang K, Liu X, Qian Y (2003) Large-scale synthesis of high quality trigonal selenium nanowires. *European Journal of Inorganic Chemistry* 2003(17):3250-3255. <https://doi.org/10.1002/ejic.200300142>
- Avendaño R, Chaves N, Fuentes P, et al (2016) Production of selenium nanoparticles in *Pseudomonas putida* KT2440. *Scientific Reports* 6:37155. <https://doi.org/10.1038/srep37155>
- Breynaert E, Bruggeman C, Maes A (2008) XANES-EXAFS analysis of se solid-phase reaction products formed upon contacting Se(IV) with FeS₂ and FeS. *Environmental Science and Technology* 42:3595–3601. <https://doi.org/10.1021/es071370r>
- Chang C, Yin R, Zhang H, Yao L (2019) Bioaccumulation and Health Risk Assessment of Heavy Metals in the Soil–Rice System in a Typical Seleniferous Area in Central China. *Environ Toxicol Chem.* ;38(7):1577–84. <http://dx.doi.org/10.1002/etc.4443>
- Chasteen TG (1993) Confusion between dimethyl selenenyl sulfide and dimethyl selenone released by bacteria. *Applied Organometallic Chemistry* 7:335–342. <https://doi.org/10.1002/aoc.590070507>
- Chasteen TG, Bentley R (2003) Biomethylation of Selenium and Tellurium: Microorganisms and Plants. *Chemical Reviews* 103(1): 1-26. <https://doi.org/10.1021/cr010210+>
- Debieux CM, Dridge EJ, Mueller CM, et al (2011) A bacterial process for selenium nanosphere assembly. *Proceedings of the National Academy of Sciences* 108 (33): 13480-13485. <https://doi.org/10.1073/pnas.1105959108>
- Dessi P, Jain R, Singh S, et al (2016) Effect of temperature on selenium removal from wastewater by UASB reactors. *Water Research* 94:146–154. <https://doi.org/10.1016/j.watres.2016.02.007>
- Doran JW (1982) Microorganisms and the Biological Cycling of Selenium. In: Marshall KC (ed) *Advances in Microbial Ecology: Volume 6*. Springer US, Boston, MA, pp 1–32
- Dowdle PR, Oremland RS (1998) Microbial oxidation of elemental selenium in soil slurries and bacterial cultures. *Environmental Science and Technology* 32(23): 3749-3755. <https://doi.org/10.1021/es970940s>
- Eswayah AS, Smith TJ, Gardiner PHE (2016) Microbial transformations of selenium species of relevance to bioremediation. *Applied and Environmental Microbiology* 82(16): 4848-4859. <https://doi.org/10.1128/AEM.00877-16>
- Eswayah AS, Smith TJ, Scheinost AC, et al (2017) Microbial transformations of selenite by methane-oxidizing bacteria. *Applied Microbiology and Biotechnology* 101:6713–6724. <https://doi.org/10.1007/s00253-017-8380-8>
- Eswayah AS, Hondow N, Scheinost AC et al (2019) Methyl Selenol as a Precursor in Selenite Reduction to Se/S Species by Methane-Oxidizing Bacteria. *Applied and Environmental Microbiology* 85(22): e01379-19. <https://journals.asm.org/journal/aem>
- Filipović N, Ušjak D, Milenković MT, et al (2021) Comparative study of the antimicrobial activity of selenium nanoparticles with different surface chemistry and structure. *Frontiers in Bioengineering and Biotechnology* 8. <https://doi.org/10.3389/fbioe.2020.624621>
- Fischer S, Krause T, Lederer F, et al (2020) *Bacillus safensis* JG-B5T affects the fate of selenium by extracellular production of colloiddally less stable selenium nanoparticles. *Journal of Hazardous Materials* 384:121146. <https://doi.org/10.1016/j.jhazmat.2019.121146>
- Haq AU, Askari S, McLister A, et al (2019) Size-dependent stability of ultra-small α - β -phase tin nanocrystals synthesized by microplasma. *Nature Communications* 10:1–8. <https://doi.org/10.1038/s41467-019-08661-9>
- Hasanuzzaman M, Borhannuddin Bhuyan MHM, Raza A, et al (2020) Selenium toxicity in plants and environment: Biogeochemistry and remediation possibilities. In *Plants* 9 (12):1–32. MDPI AG. <https://doi.org/10.3390/plants9121711>
- Hawkes WC, Alkan Z (2010) Regulation of redox signaling by selenoproteins. In *Biological Trace Element Research* 134(3): 235–251. <https://doi.org/10.1007/s12011-010-8656-7>
- Ibragimov NI, Abutalibova ZM, Agaev VG (2000) Electrophotographic layers of trigonal Se in the binder obtained by reduction of SeO₂ by hydrazine. *Thin Solid Films* 359(2):125-126. [https://doi.org/10.1016/S0040-6090\(99\)00706-3](https://doi.org/10.1016/S0040-6090(99)00706-3)
- Jain R, Jordan N, Tsushima S, et al (2017) Shape change of biogenic elemental selenium nanomaterials from nanospheres to nanorods decreases their colloidal stability. *Environmental Science: Nano* 4:1054–1063. <https://doi.org/10.1039/c7en00145b>
- Khoei NS, Lampis S, Zonaro E, et al (2017) Insights into selenite reduction and biogenesis of elemental selenium nanoparticles by two environmental isolates of *Burkholderia fungorum*. *New Biotechnology*, 34, 1–11. <https://doi.org/10.1016/j.nbt.2016.10.002>

- Komova A V, Aliev RO, Mel'nikova AA, et al (2018) Fabrication and characterization of biogenic selenium nanoparticles. *Crystallography Reports* 63:276–279. <https://doi.org/10.1134/S1063774518020098>
- Kulp A, Kuehn MJ (2010) Biological Functions and biogenesis of secreted bacterial outer membrane vesicles. In *Annual Review of Microbiology* 64:163–184. <https://doi.org/10.1146/annurev.micro.091208.073413>
- Kuršvietienė L, Mongirdienė A, Bernatoniene J, et al (2020) Selenium anticancer properties and impact on cellular redox status. *Antioxidants* 9(1):80. <https://doi.org/10.3390/antiox9010080>.
- Lampis S, Zonaro E, Bertolini C, et al (2014) Delayed formation of zero-valent selenium nanoparticles by *Bacillus mycoides* SeITE01 as a consequence of selenite reduction under aerobic conditions. *Microbial Cell Factories*, 13(1), 1–14. <https://doi.org/10.1186/1475-2859-13-35>
- Lenz, M, van Hullebusch ED, Farges F, Nikitenko S, Borca CN, Grolimund D, & Lens PNL (2008) Selenium speciation assessed by X-ray absorption spectroscopy of sequentially extracted anaerobic biofilms. *Environmental Science and Technology*, 42(20): 7587–7593. <https://doi.org/10.1021/es800811q>
- Lenz M, van Aelst AC, Smit M, et al (2009) Biological production of selenium nanoparticles from waste waters. *Advanced Materials Research* 71–73:721–724. <https://doi.org/10.4028/www.scientific.net/AMR.71-73.721>
- Lopez-Fernandez M, Jroundi F, Ruiz-Fresneda MA, Merroun ML (2020) Microbial interaction with and tolerance of radionuclides: underlying mechanisms and biotechnological applications. *Microbial Biotechnology* 14(3):810–828: <https://doi.org/10.1111/1751-7915.13718>
- Losi ME, Frankenberger WT Jr (1998) Microbial oxidation and solubilization of precipitated elemental selenium in soil. *Journal of Environmental Quality* 27(4):836–843. <https://doi.org/10.2134/jeq1998.00472425002700040018x>
- Luo X, Wang Y, Lan Y, An L, Wang G, Li M, Zheng S (2022) Microbial oxidation of organic and elemental selenium to selenite. *Science of the Total Environment* 833:155203. <https://doi.org/10.1016/j.scitotenv.2022.155203>
- Martínez FG, Moreno-Martin G, Pescuma M, et al (2020) Biotransformation of selenium by lactic acid bacteria: formation of seleno-nanoparticles and seleno-amino acids. *Frontiers in Bioengineering and Biotechnology* 8:1–17. <https://doi.org/10.3389/fbioe.2020.00506>
- Merroun ML, Raff J, Rossberg A, et al (2005) Complexation of uranium by cells and S-layer sheets of *Bacillus sphaericus* JG-A12. *Applied and Environmental Microbiology* 71:5532–5543. <https://doi.org/10.1128/AEM.71.9.5532-5543.2005>
- Minaev VS, Timoshenkov SP, Kalugin V V (2005) Structural and phase transformation in condensed selenium. *Optoelectronics and Advanced Materials-Rapid Communications* 7(4):1717–1741
- Nanchaiah Y V., Lens PNL (2015) Ecology and biotechnology of selenium-respiring bacteria. *Microbiology and Molecular Biology Reviews* 79(1):61–80. <https://doi.org/10.1128/mmb.00037-14>
- Ni TW, Staicu LC, Nemeth RS, et al (2015) Progress toward clonable inorganic nanoparticles. *Nanoscale* 7:17320–17327. <https://doi.org/10.1039/C5NR04097C>
- Ojeda JJ, Merroun ML, Tugarova A v., et al (2020) Developments in the study and applications of bacterial transformations of selenium species. *Critical Reviews in Biotechnology* 40:1250–1264. <https://doi.org/10.1080/07388551.2020.1811199>
- Otsuka O, Yamashita M (2020) Selenium recovery from wastewater using the selenate-reducing bacterium *Pseudomonas stutzeri* NT-I. *Hydrometallurgy* 197:105470. <https://doi.org/10.1016/j.hydromet.2020.105470>
- Pinel Cabello M (2021) Aplicación de tecnologías ómicas para la caracterización celular y molecular de la resistencia microbiana a uranio y selenio en la cepa *Stenotrophomonas bentonitica* BII-R7. Doctoral dissertation. University of Granada, Granada, Spain. Available in: <http://hdl.handle.net/10481/69076>
- Pinel-Cabello M, Chapon V, Ruiz-Fresneda MA, et al (2021) Delineation of cellular stages and identification of key proteins for reduction and biotransformation of Se(IV) by *Stenotrophomonas bentonitica* BII-R7. *Journal of Hazardous Materials* 418:126150. <https://doi.org/10.1016/j.jhazmat.2021.126150>
- Presentato A, Piacenza E, Anikovskiy M, et al (2018) Biosynthesis of selenium-nanoparticles and nanorods as a product of selenite bioconversion by the aerobic bacterium *Rhodococcus aetherivorans* BCP1. *New Biotechnology* 41:1–8. <https://doi.org/10.1016/j.nbt.2017.11.002>
- Presser TS (1999). Selenium pollution. In: *Encyclopedia of Environmental Science*, P. E. Alexander and R. W. Fairbridge (eds.), Springer-Verlag, Berlin, Germany, pp.554–556.

- Ranjard L, Nazaret S, Cournoyer B (2003) Freshwater bacteria can methylate selenium through the thiopurine methyltransferase pathway. *Applied and Environmental Microbiology* 69:3784–3790. <https://doi.org/10.1128/AEM.69.7.3784-3790.2003>
- Ruiz-Fresneda MA, Delgado Martín J, Gómez Bolívar J, et al (2018) Green synthesis and biotransformation of amorphous Se nanospheres to trigonal 1D Se nanostructures: Impact on Se mobility within the concept of radioactive waste disposal. *Environmental Science: Nano* 5:2103–2116. <https://doi.org/10.1039/c8en00221e>
- Ruiz-Fresneda MA, Gomez-Bolivar J, Delgado-Martin J, et al (2019) The bioreduction of selenite under anaerobic and alkaline conditions analogous to those expected for a deep geological repository system. *Molecules* 24(21):3868. <https://doi.org/10.3390/molecules24213868>
- Ruiz-Fresneda MA, Eswayah AS, Romero-González M, et al (2020) Chemical and structural characterization of Se(IV) biotransformations by *Stenotrophomonas bentonitica* into Se0 nanostructures and volatiles Se species. *Environmental Science: Nano* 7:2140–2155. <https://doi.org/10.1039/D0EN00507J>
- Sánchez-Castro I, Ruiz-Fresneda MA, Bakkali M, et al (2017) *Stenotrophomonas bentonitica* sp. nov., isolated from bentonite formations. *International Journal of Systematic and Evolutionary Microbiology* 67:2779–2786. <https://doi.org/10.1099/ijsem.0.002016>
- Sarret, G, Avoscan, L, Carrière, M, Collins, R, Geoffroy, N, Carrot, F, Covès, J, & Gouget, B. (2005) Chemical forms of selenium in the metal-resistant bacterium *Ralstonia metallidurans* CH34 exposed to selenite and selenate. *Applied and Environmental Microbiology*, 71(5), 2331–2337. <https://doi.org/10.1128/AEM.71.5.2331-2337.2005>
- Srivastava N, Mukhopadhyay M (2013) Biosynthesis and structural characterization of selenium nanoparticles mediated by *Zooglearamigera*. *Powder Technology* 244:26–29. <https://doi.org/10.1016/j.powtec.2013.03.050>
- Tugarova A V, Mamchenkova P V, Khanadeev VA, Kamnev AA (2020) Selenite reduction by the rhizobacterium *Azospirillum brasilense*, synthesis of extracellular selenium nanoparticles and their characterisation. *New Biotechnology* 58:17–24. <https://doi.org/10.1016/j.nbt.2020.02.003>
- Van Hullenbusch E, Farges F, Lenz M, Lens P, & Brown GE (2007) Selenium speciation in biofilms from granular sludge bed reactors used for wastewater treatment. *AIP Conference Proceedings*, 882: 229–231. <https://doi.org/10.1063/1.2644483>
- Vogel M, Fischer S, Maffert A, et al (2018) Biotransformation and detoxification of selenite by microbial biogenesis of selenium-sulfur nanoparticles. *Journal of Hazardous Materials* 344:749–757. <https://doi.org/10.1016/j.jhazmat.2017.10.034>
- Wang T, Yang L, Zhang B, Liu J (2010) Extracellular biosynthesis and transformation of selenium nanoparticles and application in H₂O₂ biosensor. *Colloids and Surfaces B: Biointerfaces* 80:94–102. <https://doi.org/10.1016/j.colsurfb.2010.05.041>
- Wilber CG (1980) Toxicology of selenium: a review. *Clinical Toxicology* 17:171–230. <https://doi.org/10.3109/15563658008985076>
- Winkel LHE, Vriens B, Jones GD, et al (2015) Selenium cycling across soil-plant-atmosphere interfaces: A critical review. *Nutrients* 7(6):4199–4239. <https://doi.org/10.3390/nu7064199>
- Xia X, Zhou Z, Wu S, et al (2018) Adsorption removal of multiple dyes using biogenic selenium nanoparticles from an *Escherichia coli* strain overexpressed selenite reductase CsrF. *Nanomaterials* 8:1–15. <https://doi.org/10.3390/nano8040234>
- Xu H, Barton LL (2013) Se-Bearing Colloidal Particles Produced by Sulfate-Reducing Bacteria and Sulfide-Oxidizing Bacteria: TEM Study. *Advances in Microbiology* 03(02): 205–211. <https://doi.org/10.4236/aim.2013.32031>
- Zhang J, Taylor EW, Wan X, Peng D (2012) Impact of heat treatment on size, structure, and bioactivity of elemental selenium nanoparticles. *International Journal of Nanomedicine* 7:815–825. <https://doi.org/10.2147/IJN.S28538>
- Zhao YH, Lu K, Liu T (2004) EXAFS study of mechanical-milling-induced solid-state amorphization of Se. *Journal of Non-Crystalline Solids* 356:246–251. <https://doi.org/10.1016/j.jnoncrysol.2003.12.055>
- Zhu M, Niu G, Tang J (2019) Elemental Se: Fundamentals and its optoelectronic applications. In *Journal of Materials Chemistry C* (Royal Society of Chemistry) 7(8): 2199–2206. <https://doi.org/10.1039/c8tc05873c>
- Web references**
- Lafuente B, Downs R T, Yang H, Stone N (2015) The power of databases: the RRUFF project. In: *Highlights in Mineralogical Crystallography*, T Armbruster and R M Danisi, eds. Berlin, Germany, W. De Gruyter, pp 1-30 <https://rruff.info/about/downloads/HMC1-30.pdf> (accessed December, 2021).